Available online at www.sciencedirect.com
SCIENCE DIRECT®
Journal of Nuclear Materials 321 (2003) 70–77
journal of nuclear materials
www.elsevier.com/locate/jnucmat

In situ study of the oxidation of Zircaloy-4 by ESEM

S. Abolhassani [a,*], M. Dadras [b], M. Leboeuf [b], D. Gavillet [a]

[a] *Laboratory for Materials Behaviour, Paul Scherrer Institut, 5232 Villigen-PSI, Switzerland*
[b] *Service of Microscopy and Nanoscopy, IMT, University of Neuchâtel, Jaquet-Droz, 1, 2007 Neuchâtel, Switzerland*

Received 17 September 2002; accepted 28 March 2003

Abstract

Zircaloy-4 has been oxidised in environmental scanning electron microscope (ESEM), at a temperature of 700 °C and the surface of the material has been observed during the oxidation, directly in the ESEM. The material has been subsequently analysed by atomic force microscopy (AFM) and transmission electron microscopy (TEM). Several aspects of the oxidation were revealed in these experiments. Zircaloy-4 oxidises at a different rate depending on the crystallographic orientation of the grains at the surface. The iron and chromium in the secondary phase particles (SPP) diffuse to the surface and oxidise to produce a profile at the surface of the material. The in situ observations reveal no cracks at the surface during the oxidation. Subsequent examination of the surface (ex situ) by AFM reveals the presence of pores in the oxide. TEM examinations indicate the presence of weak internal planes in the oxide layer, inducing cracks parallel to the metal–oxide interface.

1. Introduction

One of the main characteristics of zirconium and its alloys is their resistance to oxidation. Zirconium oxidises spontaneously and develops a self-healing layer of adhesive oxide. In extremely corrosive environments and at high temperatures, nevertheless, the oxidation proceeds and a uniform oxide layer forms.

The kinetics of Zr oxidation is controlled by the diffusion of oxygen ions through the existing oxide layer and the interaction with the metal at the metal–oxide interface [1]. Depending on the composition and the oxidation conditions, three crystallographic structures have been reported for the oxide: monoclinic, tetragonal and cubic zirconia [2]. The ratio of different phases is shown to vary from one material to another.

The rate of oxidation is known to depend on the composition of the material, and it follows a cubic rate law at the early stages, transforming after a so-called transition period to a linear oxidation rate. In certain alloys a cyclic cubic and linear rate laws are reported [3].

Most zirconium alloys contain precipitates (secondary phase particles, SPP) that are known to play an important role on the resistance of the material to corrosion, through anodic protection [4].

Certain aspects of the oxidation are still not clear. As an example the reason for the change of oxidation rate from cubic to linear is not well understood. If oxygen ion diffusion is the rate determining parameter throughout the process, the rate of oxidation should depend on the thickness of the oxide layer and should reduce with time. In practice this is not the case and after the so-called pre-transition period the oxidation rate raises and a linear regime is established. A linear regime implies that faster roots are available for oxygen ions to reach the interface. It is expected that pores perpendicular to the interface, or certain cracks simplify the oxygen ion access to the metal–oxide interface [5]. Studies performed by scanning electron microscopy (SEM) have shown the presence of cracks in the oxide layer, nevertheless it is not clear at what stage the cracks are produced. Also, it is not understood if these are an artefact

* Corresponding author. Tel.: + 41-56 310 2191; fax: +41-56 310 2205.
E-mail address: sousan.abolhassani@psi.ch (S. Abolhassani).

0022-3115/$ - see front matter © 2003 Elsevier B.V. All rights reserved.
doi:10.1016/S0022-3115(03)00201-0

of sample preparation or an inherent characteristic of the oxide.

In order to contribute to the understanding of the oxidation mechanism, the occurrence of cracks and the role of SPP in the oxidation of the material, attempt is made in this study to perform an in situ analysis of the oxidation by environmental scanning electron microscope (ESEM).

The objective of this observation is to examine the material's surface during the oxidation process and to monitor the phenomenon at the early stages of its occurrence.

2. Experimental

A standard Zircaloy-4 material was selected for this examination. The composition of the material is given in Table 1. The thermal treatment of the material consisted of a quench from high temperature beta phase, a heat treatment of 5 h at 500 °C, followed by a stay in the autoclave under 300 bars, at 340 °C for 32 days. These conditions are the oxidation conditions of the material when used in the pressurised water reactors (PWR). The average particle size of this sample was determined by a previous study [6] to be of the order of 30 nm. The oxide scale of this sample, obtained from the autoclave oxidation has been examined by high resolution transmission electron microscopy (HRTEM) in a previous study [7]. This material was useful since it could be considered as a specimen that can allow observing the continuation of the oxidation phenomena, if a stay at the temperature of oxidation would modify from any aspect the material.

Prior to the observation by ESEM, a fresh metallic part (without the oxide scale) was cut from the material, the surface was polished down to 250 nm, and the material was ultrasonically cleaned in order to remove all the traces of silica particles used at the last stages of polishing. For practical reasons two micro-hardness indents were produced on the surface (Fig. 1(a)), in order to have reference points for the accurate observation of the same region at different stages of heating and ESEM imaging.

A Philips XL30 ESEM-FEG was used for these experiments. The instrument was operated in ESEM mode. In the case of our experiment a water pressure of 1.3 mbar was introduced in the specimen chamber. The sample was heated at a rate of 4 °C/s allowing to reach the temperature of 700 °C in less than 3 min. The material was held for 65 min at the temperature and subsequently cooled to ambient temperature. The cooling rate of the specimen being controlled by the mass of material to be cooled, it was about 0.7 °C/s; this allowed cooling the sample to ambient temperature, in 17 min. A gas secondary electron (GSE) detector was used for the high temperature observations. At these temperatures the energy dispersive X-ray spectrometer (EDS) detector could not be used for chemical analysis. The chemical analysis of the surface was therefore performed subsequent to in situ oxidation experiment and after cooling the sample. EDAX micro-analyser was used for the chemical analysis in SEM mode.

The oxidized surface was subsequently examined by atomic force microscopy (AFM), in order to study the surface topography of the material. A Digital Instrument Nanoscope IIIa with a silicon tip was used for

Table 1
Chemical composition of Zircaloy-4 used for the experiments

Alloying elements (wt%)	Sn	Cr	Fe	Cr + Fe	O	Si (ppm)
Standard Zry-4	1.20–1.70	0.07–0.33	0.18–0.24	0.28–0.37	0.0900–0.1600	120
Zry-4 (this work)	1.30	0.10-0.11	0.22–0.23	0.33	~0.1320	100–108

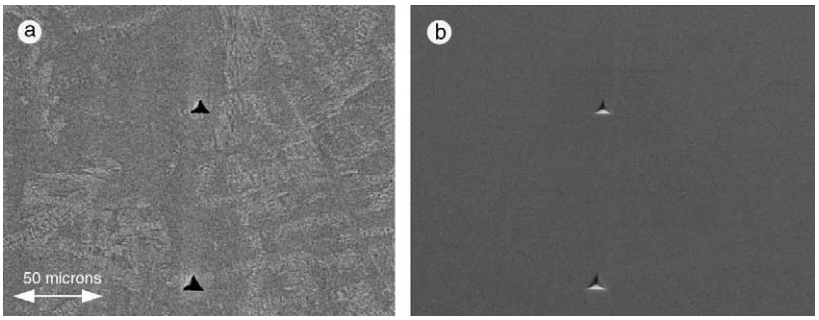

Fig. 1. The SEM images of the sample prior to heating. (a) BSE image indicating the different grains of α-zirconium. The micro-hardness indents are used to spot the region to be observed with high precision. (b) SE image of the same region indicating the topography of the surface. As can be observed from this image at this scale the surface is very smooth. Scale bar indicates 50 μm.

these observations. The tip was operated in contact mode and the AFM observations were performed at ambient temperature. In order to have a reference for the comparison of the results, the surface of a non-oxidised specimen from the same material, polished in identical conditions, was examined. AFM results of the non-oxidised surface were compared with results from the oxidised surface.

In order to examine the nature of the oxide a transverse transmission electron microscopy (TEM) sample was provided from the oxidized surface by focused ion beam (FIB). A FEI-FIB instrument was used for this specimen preparation. The TEM study of the material was performed on a JEOL 2010 with an acceleration voltage of 200 keV, equipped with a Link-ISIS energy dispersive X-ray spectrometer (EDS).

3. Results

Prior to heating, the surface of the sample was examined at different magnifications, using both secondary electron (SE) and back-scattered electron detectors (BSE). The data from the two detectors at different magnifications were complimentary and the surface topography of the material was smooth. A BSE image showing the microstructure of the beta-quenched material can be observed in Fig. 1(a). The SE image of the material at the same magnification is shown in Fig. 1(b). This image demonstrates the topography of the material at this stage.

No indication of any precipitates or any features similar to precipitates was observed on the surface prior to heating and oxidation of the material. Fig. 2(a) represents the surface of the material at higher magnification prior to oxidation. As mentioned before the sample was rapidly heated up to 700 °C. Immediately after heating, the material surface started to show small white precipitates, which were in most cases distributed in the form of a chain.

The material surface was imaged by GSE detector at regular intervals, and the following features were observed:

(a) The precipitate-like features appeared already after 3 min at 700 °C.
(b) The number of precipitate-like features that appeared at the surface did not increase considerably after the first 8–11 min of heating.
(c) The size of the precipitate-like features varied for certain larger features and remained fix for the small features.
(d) No evidence of surface cracks was observed under the conditions of observation.
(e) The material showed no further evolution after cooling to ambient temperature.

Fig. 2(b)–(d) show the material at different stages of oxidation.

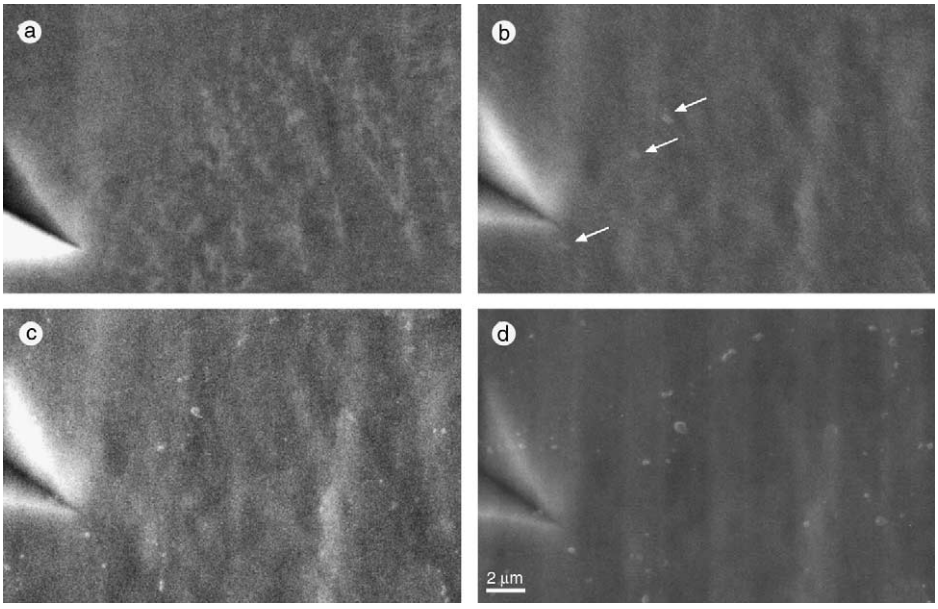

Fig. 2. In situ ESEM observation of the oxidation of the Zircaloy-4. (a) The surface before heating observed by SE detector. No precipitates are observed. (b)–(d) evolution of the surface during heating, at 700 °C, observed by GSE detector. (b) Surface after 3 min, arrows indicate first precipitates (c) after 11 min, and (d) after 62 min. The surface of the material does not show any cracks. Scale bar represents 2 μm.

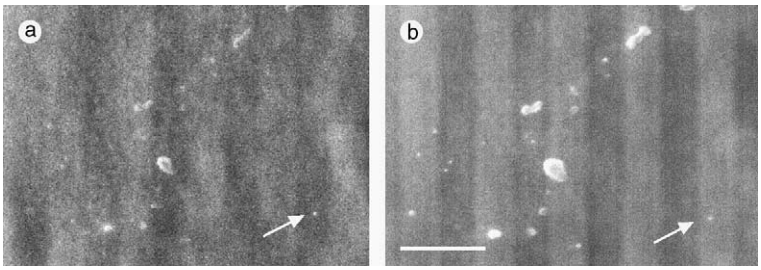

Fig. 3. In situ ESEM images of oxidation at 700 °C obtained by GSE detector, (a) after 8 min and (b) after 57 min. The number of precipitate-like features does not increase considerably after the first 8 min. However the size of larger features increases distinctly. The arrow indicates a precipitate-like feature that has not changed size after the period of oxidation. Scale bar indicates 2 μm.

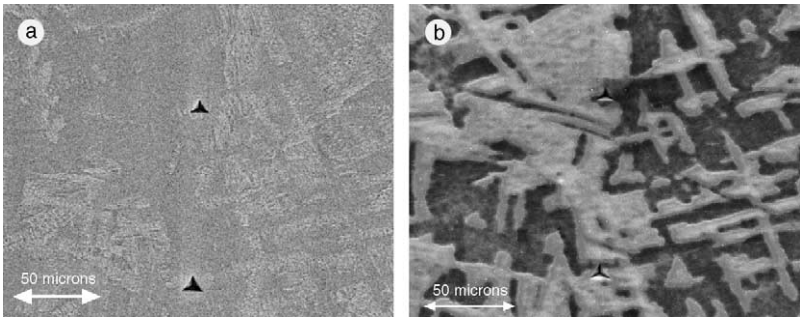

Fig. 4. The SEM images of the sample prior to heating, and after the end of the heating experiment. (a) BSE image indicating the different grains of α-zirconium prior to heating (same image as Fig. 1(a)). (b) SE image of the same region after oxidation and cooling. The dark regions in (a) have oxidised at a faster rate as can be observed in (b). The micro-hardness indents can be used to locate same grains before and after oxidation. Scale bars indicate 50 μm.

A better comparison of the evolution of the surface features is possible in Fig. 3. As mentioned above, the number of precipitate-like features formed after 8 min in situ oxidation (Fig. 3(a)) does not increase considerably after 57 min of oxidation (Fig. 3(b)). Nevertheless the size of large features increases distinctly with time; this is not the case for the smaller features. The analysis of the surface of the material during the experiment does not reveal the occurrence of any cracks during the oxidation period.

After cooling the examination of the surface of the material indicated that the rate of oxidation has been different for various parts of the material, and a clear topography representing the microstructure of the material can be noticed. Fig. 4(b) represents this phenomenon; the comparison with Fig. 4(a) reveals well this feature. As it can be observed the darker regions of image 4(a) have produced a profile that stands higher than the regions appearing bright prior to oxidation. The topography can be compared with Fig. 1(b). At the same magnification the surface reveals the considerable change of topography of the material after oxidation.

At higher magnifications the precipitate-like features can be observed. Fig. 5 reveals the distribution of precipitates in the material. A detailed examination of the surface showed that the distribution of precipitates in the different regions at the surface is similar.

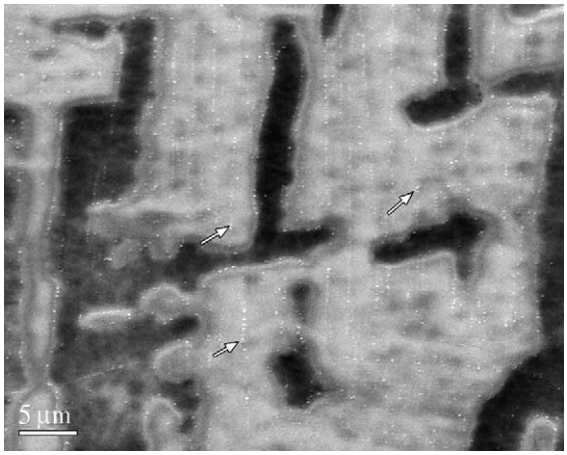

Fig. 5. The oxidised and cooled material reveals the microstructure of the metal substrate as well as the distribution of the secondary phase particles (arrows). Scale bar represents 5 μm.

In order to examine the nature of the precipitate-like features, certain larger features were analysed by EDS and compared to the matrix (Fig. 6). The results

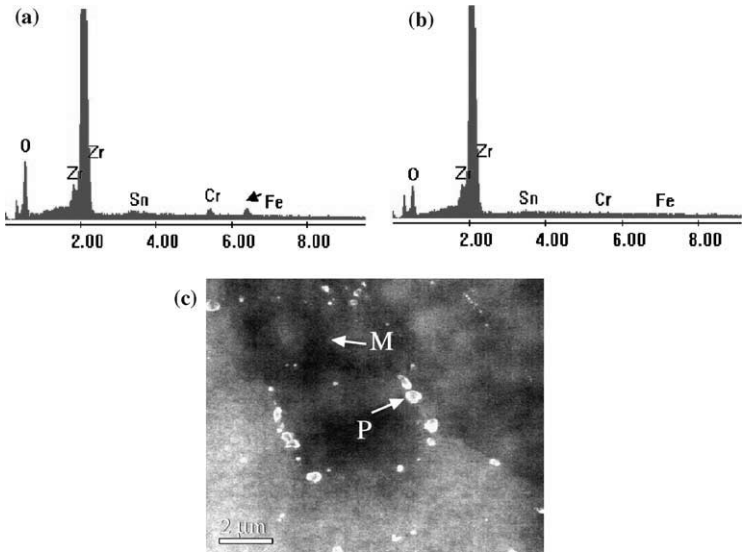

Fig. 6. The EDS analysis of a precipitate-like feature (a) and of the matrix (b) by SEM, the image (c) indicates the region of analysis. P: precipitate, M: matrix.

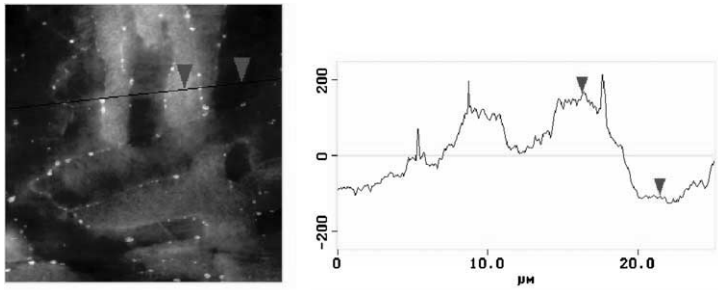

Fig. 7. (a) AFM image of the topography of the surface after oxidation. The oxidised precipitates are protruding from the surface of the matrix oxide. The topography of the surface confirms the fact that the oxidation rate is different for zirconium grains oriented differently with respect to the surface. The z scale is 492 nm; the total scanned area is 25μm. (b) The z profile of the line indicated in (a). The height difference between the points indicated by the arrows is 267 nm. In this profile three precipitates are included forming the spikes. The profile indicates that the z-values of the precipitates are above the surrounding matrix oxide.

indicated without ambiguity that the features do contain Fe and Cr, whereas the matrix did not show any signal from these two elements.

Fig. 7 represents the overall image of the material after cooling, obtained by AFM. The height difference, between the highest and the lowest surface regions, is shown in the line profile. In this measurement, the height difference between the two grains is measured to be of the order of 250 nm. From this profile it can be seen that the precipitates are protruding from the matrix oxide. Precipitates in all regions show a z-value that is above their surrounding matrix. It can be observed that the precipitates are mostly at the boundary of the two regions (grain boundaries) and the height of precipitates is of the order of 50–90 nm above the oxide surface. The topography of the metal at a polished state and without any in situ oxidation is much smoother than after oxidation. The AFM height variation between two grains in this case, in the same magnification, is measured to be in the range of 50 nm (not shown here).

A smaller region of the surface is observed by AFM (Fig. 8) and the results reveal that the morphology of the oxide is granular. At this scale oxide grains as small as 35 nm are observed. At some regions of the surface evidence of pores are noticed, these pores seem to be randomly distributed and their size and geometry are not uniform.

Fig. 9 indicates a TEM bright field image of the transverse section of the specimen, in the metal–oxide region. This TEM sample was cut in the direction perpendicular to the oxidised surface and attempt was made

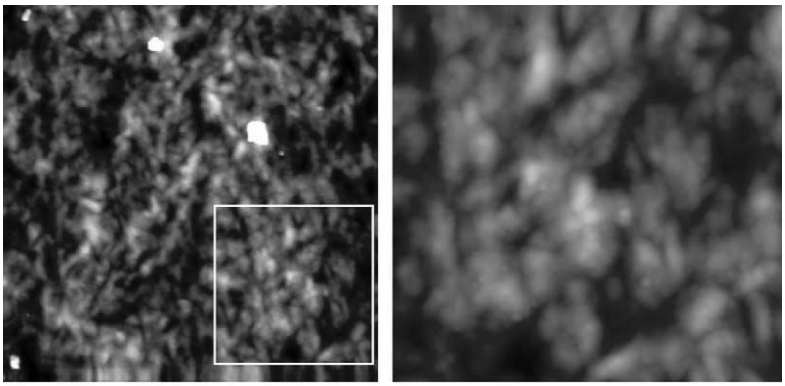

Fig. 8. AFM images of the topography of the surface after oxidation. (a) Total scanned area is 5 μm and the z scale is 82 nm. (b) The region framed in (a) scanned again (total scanned area is 2 μm), z scale is 88 nm.

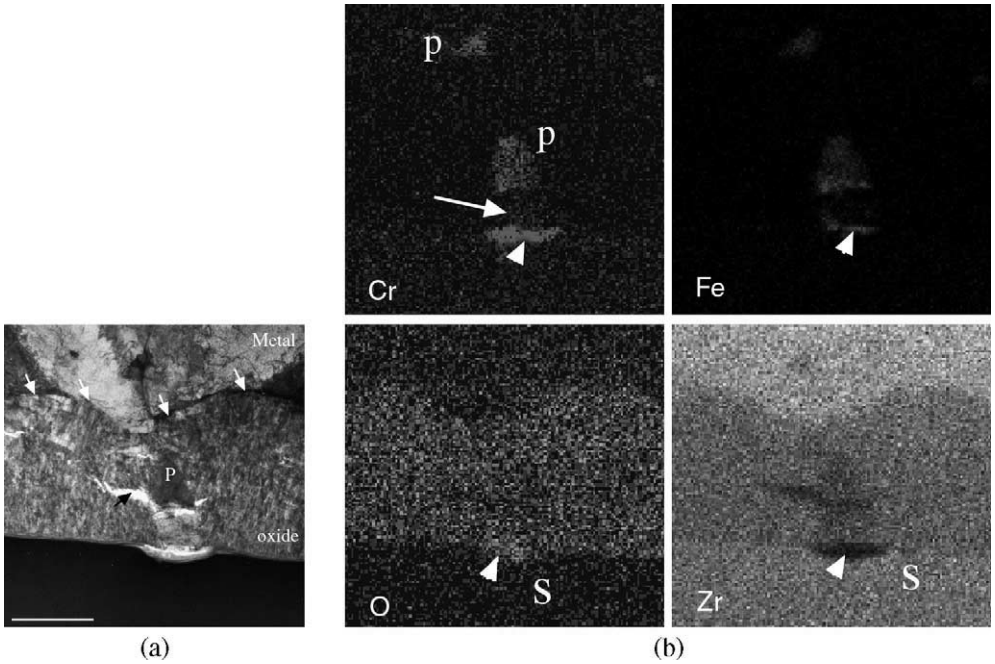

Fig. 9. (a) TEM bright field image of the metal–oxide interface showing a precipitate in the oxide region. At the surface of the oxide a lens-type feature is observed. This corresponds to the precipitate-like features observed in ESEM and AFM. The thickness of this lens is about 130 nm and the width of the lens is 700 nm. Cracks are observed at the vicinity of the precipitate. P designates the precipitate in the oxide, white arrows indicate the interface, and black arrow indicates the crack. Scale bar represents 1000 nm. (b) EDS maps of Cr (blue), Fe (red), O (green), and Zr (yellow) in the same region as in (a). As it can be observed in the map of Cr and Fe, very little signal from these elements, is present in the region between the precipitate and the outer surface of the oxide. The lens region however contains no Zr, but shows a signal from Cr, Fe and oxygen. P designates precipitate (in the oxide and also in the metal), arrow indicates the region between the precipitate and the free oxide surface, arrow heads indicate the lens at the surface of the oxide and S indicates the free space above the oxide.

to include a precipitate in the thin film. This precision of sample preparation is only possible by FIB. The precipitate and the EDS maps of chromium, iron, oxygen and zirconium, of the same region are shown. As it can be seen in the EDS maps, there is very little signal from Cr or Fe in the region between the precipitate and the outer oxide surface. The protruded region at the surface of the oxide does not contain any Zr. Since the intermetallic precipitates are in the form $Zr(Fe/Cr)_2$ and must contain a considerable amount of Zr, this observation

demonstrates that Fe and Cr have diffused to the surface of the material. The oxygen map shows that the Cr and Fe at the surface are in oxide form. From this observation it is concluded that a precipitate-like feature could be the result of the diffusion of the species in the precipitate to the surface of the material and does not represent necessarily the precipitate itself.

From the measurements on the TEM sample, the average oxide thickness was found to be 1.6 μm. The crystal structure of the oxide has been examined by TEM and by X-ray powder diffraction analysis to be monoclinic; a residual amount of tetragonal phase has been observed by the second technique.

4. Discussion

It must be noted that the ESEM in situ experiment is a surface analytical method; in other terms it reveals the changes occurring at the surface of the material, and it will not bring any information from the internal interfaces. However, in this work it is combined with complementary ex situ experiments to provide a useful tool for the examination of the oxidation phenomena. From the in situ observations and subsequent ex situ experiments some aspects of the oxidation can be revealed, as discussed below.

One of the phenomena observed during the oxidation of Zircaloy materials is the nodular corrosion of alloys containing precipitates [8]; this behaviour has been correlated to the presence of the intermetallic precipitates. Nevertheless the correlation is still not unambiguously demonstrated. The precipitates in the case of Zircaloy-4 and Zircaloy-2 are claimed to be electrochemically less reactive than the Zr matrix and therefore do not interact with oxygen so long as they are in contact with the metallic Zr. Once the precipitates are no more in contact with the Zr matrix, they start corroding [9].

From the present observation, it can be concluded that the oxidation of the precipitates when started, induces a layer of oxide at the surface, which contains very little Zr. This phenomenon results from the diffusion of Cr and Fe to the free surface of the material and a subsequent interaction with oxygen. Fig. 9 indicates this phenomenon. As it can be seen the protruding material at the surface is responsible for the lens formation as shown in Fig. 2, and in AFM images. The occurrence of these features is at the origin of the nodules on the surface of the oxide.

From the occurrence of precipitate-like features at the very early stages of oxidation (please see Figs. 2(b) and 3(a)), it can be concluded that the oxidation at the surface takes place simultaneously for the matrix and the precipitates. Once the surface precipitates were all oxidised the number of precipitates at the surface did not increase any further. This would imply that either the diffusion path for precipitates below the surface was too long for the time period of the test, or that the phenomenon does not continue after the oxidation of precipitates near the surface.

Another parameter that could be responsible for this phenomenon is the grain boundary diffusion of Fe and Cr. As most of the precipitates in this material are at the grain boundaries, it is possible that such a lens formation is due to the grain boundary diffusion of these species. This question should be further examined with other experiments.

The stresses leading to the formation of cracks in the oxide can have at least three origins: (a) they can be due to the volume differences between the oxide and the metal, (b) they can be of thermal origin owing to the difference of expansion coefficients of the oxide and the metal and (c) they can be due to the changes in the structure of the oxide during oxidation [10,11]. The fact that no cracks are observed at the surface of the oxide during the in situ experiment does not necessarily imply that there are no cracks in the bulk oxide. However, this observation implies that the oxide surface does not show large flaws, and therefore no large paths for the access of the oxidising species to the interface are created from the surface. The presence of pores revealed by AFM studies implies however that there are other roots than the bulk diffusion of oxygen ion for reaching the interface.

The expansion coefficient of zirconia both in monoclinic and tetragonal phases is anisotropic, in the case of the monoclinic phase it ranges between 1.2×10^{-6} K^{-1} for the [0 1 0] directions and 12.6×10^{-6} K^{-1} for the [0 0 1] direction. As the expansion coefficient of the metallic Zr is about 5.6×10^{-6} K^{-1}, it would be expected that the large difference in thermal expansion would induce cracks in the oxide during the cooling [12] The absence of cracks on cooling could be explained by the size and orientation of oxide grains, and the distribution of stresses at the temperature of oxidation. In other words the mechanical behaviour of the metal–oxide system reflects the geometry and crystal orientation at microscopic level of that system.

The process temperature of 700 °C will induce an oxidation rate that is faster than the rates observed in the PWR (at about 340 °C). This temperature was selected in the present study, in order to perform the experiment within a time frame that can be realistic for the use of the ESEM instrument. It is assumed that under such conditions only the rate of oxidation will change. The rate of cooling of this sample being very fast, the thermal shock is expected to induce cracks in the oxide. However, no cracks are observed during cooling, on the surface of the material. This observation can be extrapolated to lower temperature conditions and it can be concluded that the thermal stresses in this material do not induce any cracks at the surface of the material,

during the cooling for the stage of the oxidation attained by the experiment. This observation should be used with precaution for other materials and it is preferable to verify this behaviour for other materials before the extrapolation of the results.

The role of precipitates in the modification of the stress distribution in the oxide layer has not yet been analysed. As can be observed in Fig. 9 a crack is present in the vicinity of the precipitate. Such cracks have been observed in other cases and could imply a stress build-up near the precipitate, when this latter starts to oxidise. It is clear that these cracks being parallel to the interface and under the surface of the oxide, it is not possible to check whether they are produced during the in situ experiment or later during the specimen handling. Even if the cracks are produced during the handling, they reveal the weakness of the material in these points. Work is in progress to further clarify this subject.

The dependence of the oxide thickness to the grain orientation is explained by crystallographic but also by compositional effects. This is in agreement with the observation of previous authors [13,14].

5. Conclusions

The results from in situ and ex situ observations have shown that:

No precipitate can be revealed with the SEM for the material studied, prior to oxidation of the material. Near the surface, and from very early stages of in situ oxidation, iron and chromium present in the precipitates diffused to the surface, to produce a lens type oxide.

During the in situ oxidation of the material at 700 °C, no cracks are observed at the surface.

The rapid cooling of the material from 700 °C to room temperature induces no cracks on the surface of the material.

Under identical conditions of oxidation, the rate of oxidation depends on the crystallographic orientation of the grains and on the microstructure of the material. In the present study this observation was confirmed and quantified by AFM topographic measurements.

In the vicinity of the precipitates, cracks are observed by TEM in the direction parallel to the interface. These cracks are nevertheless not observable at the surface, during the in situ experiment.

Acknowledgements

The authors wish to thank Dr R. Münch for supplying the autoclaved Zircaloy-4. Dr C. Jiao from FEI-UK is acknowledged for the FIB sample preparation.

References

[1] A. Grandjean, Y. Serruys, J. Nucl. Mater. 273 (1) (1999) 111.
[2] M. Inagaki, M. Kanno, H. Maki, Proceedings of the 9th International Symposium: Zirconium in the Nuclear Industry, ASTM STP 1132, American Society for Testing and Materials, Philadelphia, 1991, p. 437.
[3] H. Anada, K. Takeda, S. Hagi, T. Murata, A. Oe, T. Miyashita, Proceedings of the ANS International Topical Meeting on LWR Fuel Performance, IAEA, Park City, 2000, p. 445.
[4] T. Isobe, T. Murai, Y. Mae, 11th International Symposium: Zirconium in the Nuclear Industry, ASTM STP 1295, American Society for Testing and Materials, Garmisch-Partenkirchen, 1996, p. 203.
[5] B. Cox, Y.M. Wong, J. Nucl. Mater. 270 (1–2) (1999) 134.
[6] R.K. Münch, Application of the electrochemical impedance spectroscopy method to the study of the growth of Zircaloy oxides at high temperature and high pressure, PhD thesis, Lausanne, EPFL, 2000.
[7] S. Abolhassani, R. Schäublin, F. Groeschel, G. Bart, Proceeding of Microscopy and Microanalysis 2001, Long Beach, California, USA, 5–9 August 2001, p. 250.
[8] D. Franklin, C.-Y. Li, in: R.B. Adamson, L.F.P. Van Swam (Eds.), Zirconium in the Nuclear Industry: Seventh International Symposium, ASTM STP 939, American Society for Testing and Materials, Philadelphia, 1987, p. 206.
[9] J.H. Baek, Y.H. Jeong, J. Nucl. Mater. 304 (2002) 107.
[10] T. Jacquot, R. Guillen, M. François, B. Bourniquel, J. Senevat, Mater. Sci. Forum. 228–232 (1996) 845.
[11] H.G. Weidinger, H. Ruhmann, G. Cheliotis, M. Maguire, T.-L.Yau, in: C.M. Eucken, A.M. Garde (Eds.), Zirconium in the Nuclear Industry: Ninth International Symposium, ASTM STP 1132, American Society for Testing and Materials, Philadelphia, 1991, p. 499.
[12] N. Pétigny, P. Barberis, C. Lemaignan, C.H. Valot, M. Lallemant, J. Nucl. Mater. 280 (2000) 318.
[13] G. David, R. Geschier, C.J. Roy, J. Nucl. Mater. 38 (1971) 329.
[14] H.G. Kim, T.H. Kim, Y.H. Jeong, J. Nucl. Mater. 306 (2002) 44.